nature chemical biology

Article

https://doi.org/10.1038/s41589-026-02254-6

Early maturation of host antimicrobial peptide defences is associated with host–pathogen coexistence

Received: 11 April 2025

Accepted: 22 May 2026

Published online: 15 July 2026

Check for updates

Phillip A. Jervis[1,2,3], Gonçalo M. Rosa[1,4,5], Kieran A. Bates[1,6], Kersti Karu[3], Aamina Murtza[3], Thomas Defuentes[3], David Firer[7,8], Sam Edwards[9,10,11], Kevin Hopkins[1], François Le Mauff[7,8], Christopher J. Michaels[12], Tresai Jordine-Morgan[1], Christina Nylander[3], Christopher Sergeant[1], Emily J. Skelly[1,2], Tam T. Bui[13], Donald Sheppard[7,8], Xavier A. Harrison[14], Johanna Rhodes[2,15,16], Benjamin Tapley[12], Jaime Bosch[4], Trenton W. J. Garner[1,17] ✉, Matthew C. Fisher[2] ✉ & Alethea B. Tabor[3] ✉

Epizootic outbreaks of invasive pathogens, such as the fungal pathogen *Batrachochytrium dendrobatidis* (*Bd*), are increasingly recognized as a global threat to biodiversity. However, not all susceptible host populations are equally impacted by these disease outbreaks. While some populations persist despite intense infections and high mortality rates, others can transition to enzootic coexistence with the pathogen. Here, we use comparative peptidomics to identify differences in antimicrobial peptide (AMP) maturation in *Bd*-susceptible common midwife toads (*Alytes obstetricans*) through metamorphosis. Here, we show that animals that metamorphose before AMP immune maturation display a low-diversity AMP phenotype deficient in anti-*Bd* AMPs. Where a high incidence of postmetamorphic animals occur with immature AMPs, populations are associated with epizootic disease dynamics. Conversely, populations associated with mature AMPs are stable following invasion of the pathogen. Our results show that even intrinsically susceptible amphibian species can possess the tools that allow populations to recover following a severe *Bd* epizootic.

When highly transmissible pathogens are introduced into a naive community of susceptible hosts, these often experience one or a series of epizootic waves[1]. Over time, barring extinction of the pathogen or the host, epizootic disease dynamics will usually subside into more stable enzootic equilibria. Divergent trajectories and asynchronous rates of recovery can generate contemporary patterns of epizootic and enzootic disease dynamics between persisting host populations[2,3]. Comparative studies between these populations can offer insights into the role of host immunity in shaping population-level disease outcomes[4]. Antimicrobial peptides (AMPs) are a crucial and near-ubiquitous component of innate immune defense across the tree of life[5] and have been shown to inhibit the growth of bacterial, viral and fungal taxa in vitro[6]. Innate immune effectors, including AMPs, are traditionally considered a primitive, broad-spectrum antimicrobial barrier for preventing infection[7]. Despite this long-held perception, there is a growing body of work challenging this oversimplification[5,8]. While the innate immune system does constitute the first line of defense against novel pathogens, the complexity and specificity of the constituent AMPs has been long overlooked.

As anthropogenically spread emerging infectious diseases (EIDs) increasingly impact humans, agriculture and wildlife[9], there is a pressing need to understand the interactions between host immunity and

A full list of affiliations appears at the end of the paper. ✉e-mail: Trent.Garner@ioz.ac.uk; matthew.fisher@imperial.ac.uk; a.b.tabor@ucl.ac.uk

https://doi.org/10.1038/s41589-026-02254-6

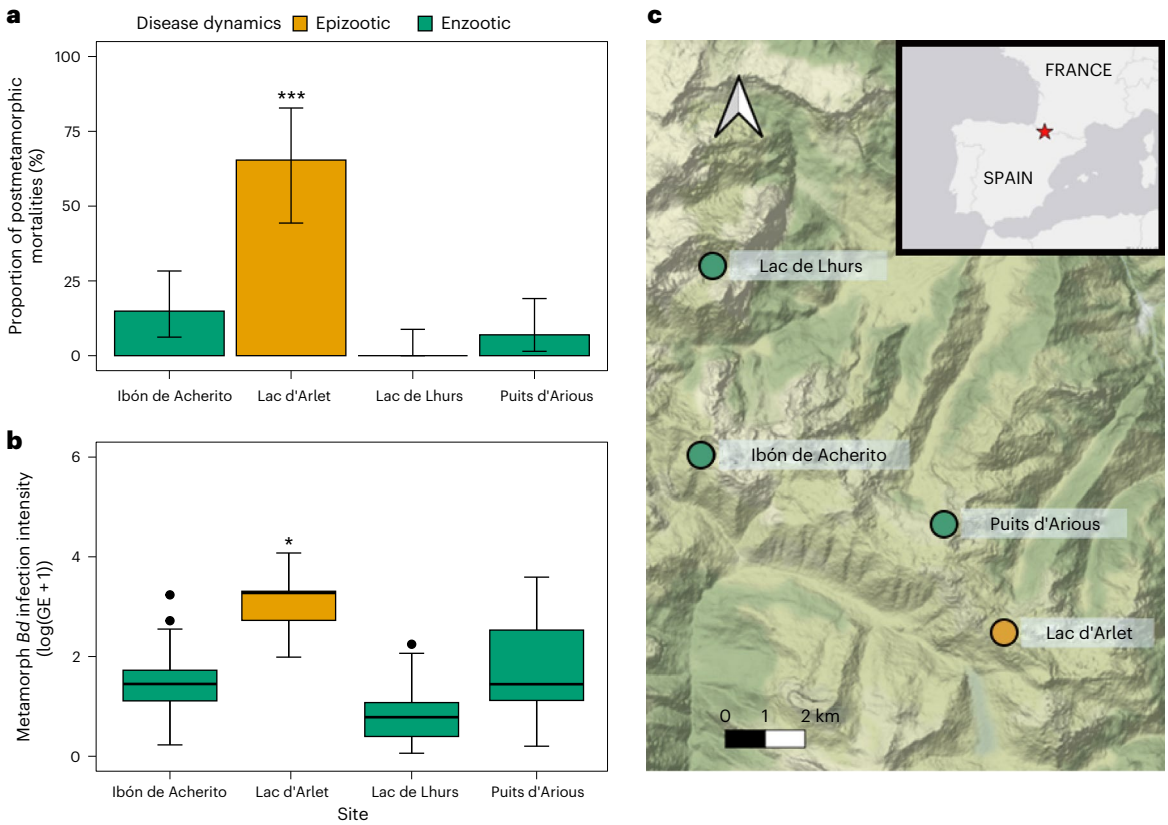


Fig. 1 | Post metamorphic *Bd* disease dynamics in the Western Pyrenees. **a**, Proportion of deceased postmetamorphic individuals (Ibón de Acherito, $n = 7$; Lac d'Arlet, $n = 17$; Lac d'Lhurs, $n = 0$; Puits d'Arious, $n = 3$) from total encountered (Ibón de Acherito, $N = 47$; Lac d'Arlet, $N = 26$; Lac d'Lhurs, $N = 40$; Puits d'Arious, $N = 43$) during field surveys. Significance was determined by Kruskal–Wallis test ($\chi^2(3) = 58.497$, $P < 0.001$), followed by a pairwise, two-sided Fisher's exact test with Hochberg correction for multiple comparisons ($P < 0.001$). Error bars are Clopper–Pearson confidence intervals at 95% confidence. **b**, Box plot showing that the infection intensity of *Bd*-positive animals ($n = 5$) at Lac d'Arlet (Epizootic) is significantly higher than infection burdens in the enzootic populations (Ibón de Acherito, $n = 33$; Lac d'Lhurs, $n = 30$; Puits d'Arious, $n = 38$). Significance was determined using a Kruskal–Wallis test, followed by a pairwise, two-sided Wilcoxon test. **c**, Map of field sites. All individuals represent biological replicates. The box plot shows the median (center), 25th and 75th percentiles (box limits) and 1.5× the interquartile range (whiskers). Significance is denoted by $^*P < 0.05$, $^{**}P < 0.01$ and $^{***}P < 0.001$. The map image is the intellectual property of Esri and its licensors and is used herein under license (Copyright © 2021 Esri and its licensors).

these novel pathogens. Here, the amphibian-infecting chytrid fungus, *Batrachochytrium dendrobatidis* (*Bd*), is one of the most impactful EIDs known and is a recognized threat to amphibian diversity worldwide[10]. Chytridiomycosis, the disease caused by *Bd*, causes acute epidermal disruption, leading to pathophysiological changes associated with high rates of mortality in susceptible species[11]. The resulting population declines have been monitored over the past forty years and the loss of amphibian taxa, particularly in tropical montane ecosystems, results in the loss of ecosystem function[12,13] and the collapse of predator communities through trophic cascades[14]. Despite these localized catastrophic events, at a global level, the emergence of *Bd* is associated with heterogeneous patterns of declines of susceptible amphibians at both interspecific[11] and intraspecific levels[2,3].

There is some evidence to suggest that increased host immunity is contributing to the persistence of susceptible host populations[11,15]. As a pathogen of amphibian skin, *Bd* must first survive contact with the epidermal mucosal layer before it can infect the host. Variation in the efficacy of these mucosal defenses may explain the observed heterogeneity in population-level responses to a *Bd* epizootic. The highly diverse mixtures of both host[16] and microbial compounds[17] present in the mucosal layer have been shown to inhibit the growth of *Bd* in vitro[18] and in vivo[15]. AMPs, in particular, are thought to be a critical component of an amphibian's mucosal innate immune defense against pathogens such as *Bd*. This hypothesis owes much to previous in vitro work showing increased anti-*Bd* efficacy of mucosal samples from resistant amphibian species and the corresponding in vitro activity of synthetic amphibian AMPs[19]. However, there has been substantial difficulty in linking these in vitro AMP experiments to population-level studies in the field.

In many amphibian species, the metamorphosis from the larval to postmetamorphic stages carries an elevated risk of mortality from chytridiomycosis[20]. This elevated risk is generated through two simultaneous developmental processes, keratinization of the skin and immune maturation. As a keratinophilic parasite, *Bd* requires keratinized amphibian skin as a substrate for its survival in vivo[21]. In fatal chytridiomycosis, the osmoregulatory capacity of the amphibian's skin breaks down, leading to cardiac asystolic death through electrolyte imbalance[11]. However, tadpoles do not possess keratinized skin[22]. Whilst *Bd* can infect their keratinized mouthparts, this does not develop into chytridiomycosis and is generally not fatal[23]. During metamorphosis, as keratinization of the skin occurs, the pathogen can spread to the skin, which can then develop into chytridiomycosis. This transition from a *Bd*-tolerant to a *Bd*-susceptible life stage coincides with a critical period of immune reorganization[24]. The immune system of tadpoles is considered immature and less effective in comparison to postmetamorphic animals[25]. At an organismal level, the development of the constitutive, innate and adaptive immune defenses takes places at discrete stages before, during and after metamorphosis as the requisite organs develop[26]. At a skin level, the AMP repertoire of tadpoles is considerably different to postmetamorphic life stages[25,27], with

https://doi.org/10.1038/s41589-026-02254-6

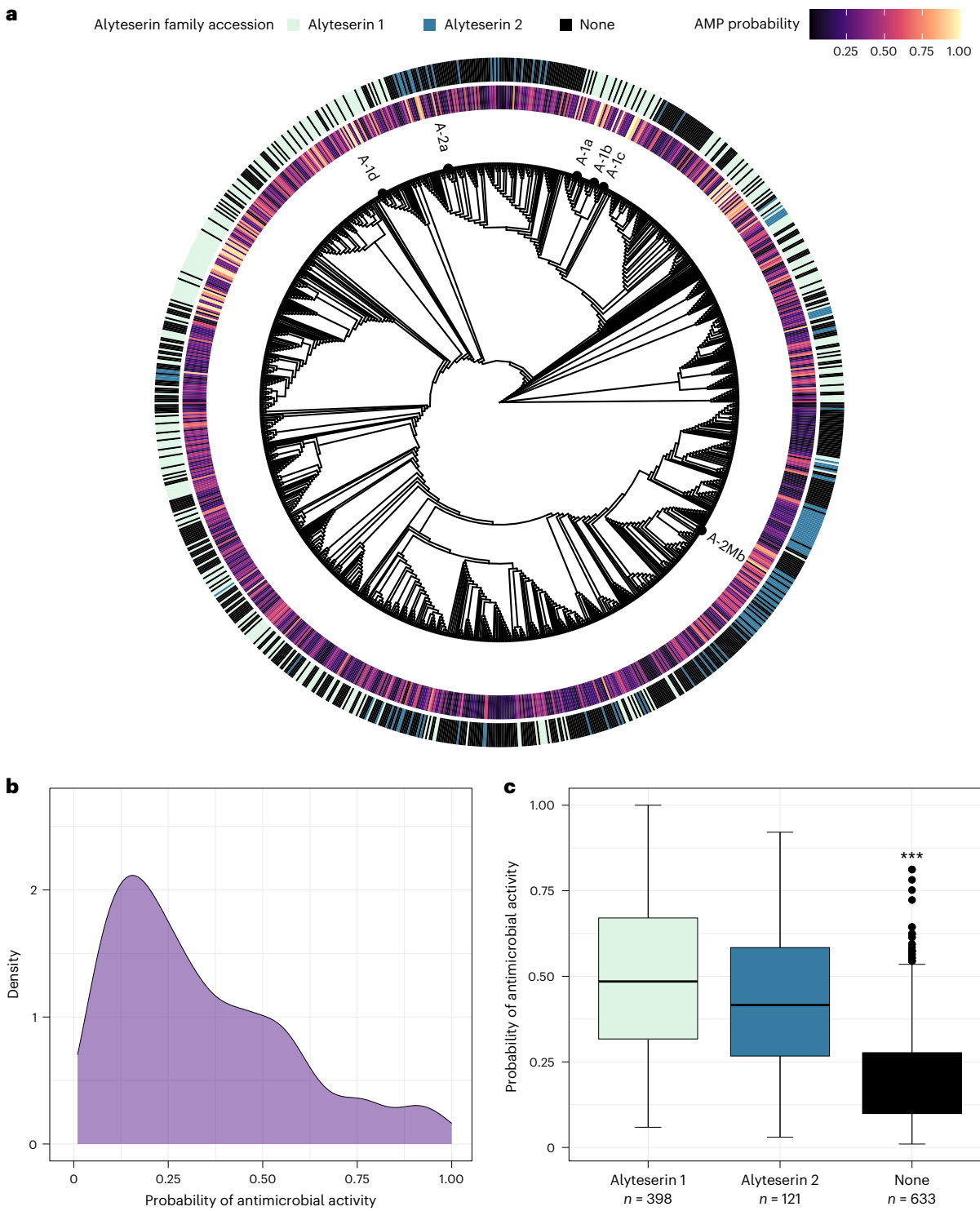


Fig. 2 | Peptidomic characterisation of skin-secreted peptides in *A. obstetricans*. **a**, Cladogram showing the 1,152 mucosal peptides characterized from the field data. Known AMPs are annotated. The inner heat map indicates the probability that each sequence has antimicrobial activity (as predicted by MACREL AMP prediction tool). The outer heat map shows alignment of each peptide to alyteserin AMP family. **b**, Frequency distribution of the probability of AMP activity predicted by MACREL. **c**, Box plot showing significantly lower predicted antimicrobial activity of peptides not aligned to alyteserin-family AMPs. Significance was determined using a Kruskal–Wallis test ($\chi^2(2) = 448.83$, $P < 0.001$), followed by a pairwise, two-sided Wilcoxon test with Benjamini–Hochberg correction for multiple comparisons ($P < 0.001$). The box plot shows the median (center), 25th and 75th percentiles (box limits) and 1.5× the interquartile range (whiskers). Significance is denoted by $^*P < 0.05$, $^{**}P < 0.01$ and $^{***}P < 0.001$.

further changes potentially occurring between recent metamorphs and sexually mature adults[28]. The inhibitory potential of these limited AMP defenses in larval amphibians has been reported to be significantly lower than those of postmetamorphic animals[27]. However, there has been no research into the population-level variation of these immune profiles across life stages in nature.

The common midwife toad (*Alytes obstetricans*) is susceptible to *Bd* but its population-level response to *Bd* introduction has been

https://doi.org/10.1038/s41589-026-02254-6

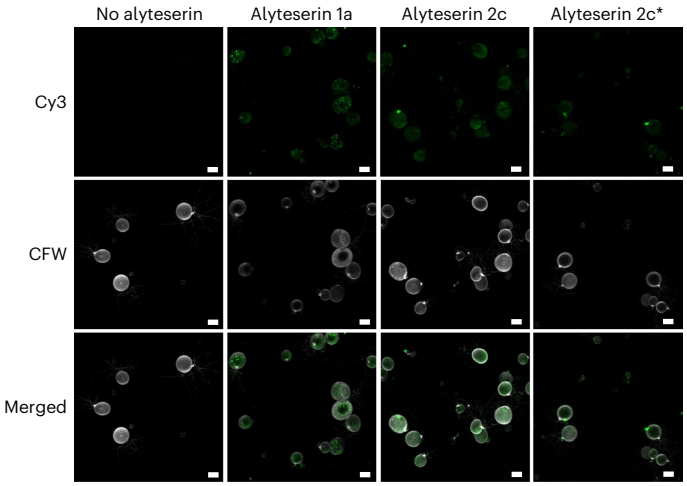


Fig. 3 | Confocal microscopy experiment of *Bd*-GPL isolate IA042 challenged with Cy3-labeled peptides. The four treatments were negative control, Cy3–alyteserin 1a, Cy3–alyteserin 2c and Cy3–alyteserin 2c (scrambled sequence). Imaging channels shown are Cy3 (alyteserin AMP, green) and Calcofluor white (cell walls, white) and the merged channel of both dyes. Imaging shows that alyteserins interact with *Bd* through an intracellular mechanism. The asterisk indicates scrambled peptide sequence. Scale bar, 10 µm. Each experiment was repeated twice and the same observations were made in both experiments.

highly variable[2,29–31]. This species is particularly susceptible to chytridiomycosis during or shortly after metamorphosis, often leading to seasonal mass mortality events in montane regions[31]. In the Western Pyrenean Mountain range, all populations of *A. obstetricans* experienced heavy declines following *Bd* introduction, yet four of these populations have persisted 19 years later, with three transitioning to stable, enzootic disease dynamics[2]. At Lac d'Arlet, one population continues to exhibit epizootic dynamics characterized by high *Bd* infection intensity, seasonal mass mortality events and near extirpation. This observed heterogeneity in disease dynamics is known to be associated with amongst-lake variation in host microbiome[2,4]; however, an underlying immunological mechanism driving these host–microbe interactions is missing.

Here, we aimed to investigate the extent to which the observed disease dynamics were associated with variation in host AMP defenses. The AMP defenses of *A. obstetricans* include the alyteserin family, which consists of 12 cationic, α-helical cytolytic AMPs that are C-terminally amidated[32]. However, it remains unknown whether some or all the known alyteserins inhibit *Bd* or whether they could operate synergistically as is the case in other amphibian AMP systems[33,34]. If there is variation in anti-*Bd* efficacy between AMPs, then population-level responses to chytridiomycosis could occur through differences in composition or concentration of their AMP arsenal.

Since the description of the alyteserin AMPs in *A. obstetricans* in 2009, recent advances in mass spectrometry (MS)-based proteomics[35,36], when integrated with transcriptomic references, has allowed for the high-throughput characterization of complex peptidomic mixtures. While these methods are typically used in human health research[37,38], we were able to apply these analytical techniques to this wild amphibian disease system. In combination with molecular diagnostics, in vitro AMP *Bd* inhibition assays and confocal microscopy, we leveraged a multidisciplinary approach to investigate whether these differences in contemporary disease dynamics in the Western Pyrenees are associated with (1) the composition and efficacy of host AMP defenses in recently metamorphosed animals; (2) preinvestment in AMPs at the larval stage; and (3) the varied epidemiological outcomes that we observe across this long-term study system.

Results

We confirm the continuation of epizootic disease dynamics, characterized by high levels of mortality (Fig. 1a) and infection intensity (Fig. 1b), in recently metamorphosed *A. obstetricans* at Lac d'Arlet. While this population has continued to persist despite many years of heavy chytridiomycosis-driven mortality, the low numbers of postmetamorphic individuals found during surveys (2019: $n = 2$, 2020: $n = 7$) relative to the enzootic populations (Ibón de Acherito, Puits d'Arious and Lac de Lhurs) shows that the population has yet to successfully coexist with the introduced pathogen.

The mucosal peptidome is a highly diverse immunophenotype

We sampled skin secretions from a total of 154 *A. obstetricans* tadpoles and 123 postmetamorphic individuals across the four survey sites. Peptidomic analysis of the samples was then carried out by liquid chromatography (LC)–MS/MS under conditions that allowed for detection and sequencing of all peptide components. To identify these peptides, we performed a peptidomic workflow in PEAKSStudio12 (Bioinformatic Solutions). In summary, de novo peptide sequences went through a two-round database search (first against the AMP database (APD3 database[39]) and then against a skin transcriptome reference library generated from captive *A. obstetricans*). All unaligned sequences were then assembled into de novo features using the DeepNovo algorithm[40], before quality filtering and quantification of all identified peptide features. We found that the mucosal peptidome of *A. obstetricans* skin is far more diverse than the existing literature suggests (Fig. 2a)[32]. The field mucosal peptide samples yielded 1,820 putative peptides (inclusive of post-translational modifications), with 1,152 of these peptides passing the quality filtering stage for label-free quantification (Fig. 2a). Amongst these peptides are six previously described alyteserin AMPs (Supplementary Table 1)[32]. We also found alyteserin 2 Mb, which was only previously described in the closely related *A. maurus*[41]. Overall, from the 1,152 secreted mucosal peptides, the majority of these peptides were not predicted to have antimicrobial activity (Fig. 2b) by the MACREL AMP prediction tool[42] (mean probability of AMP activity: 0.34, range: 0.01–1, s.d.: 0.24).

To enrich the dataset for peptides likely to possess antimicrobial activity, we removed peptide sequences without significant ($-\log P > 20$) alignment to alyteserin 1 or alyteserin 2 AMPs (Fig. 2c). These removed sequences were predicted to have a significantly lower probability of AMP activity (Kruskal–Wallis: $\chi^2(2) = 448.83$, $P < 0.001$; pairwise Wilcoxon test: $P < 0.001$). A surprisingly large number of peptides had alignment with alyteserin 1 ($n = 398$) or alyteserin 2 ($n = 121$) AMPs, which is far higher than expected given the limited diversity of reported AMPs in the species. Much of this diversity appears to have been introduced after translation. This variation includes C-terminal acid and C-terminal amide analogs of all alyteserin AMPs, fragments of alyteserin AMPs and likely variation in the cleavage site from the propeptide observed as additional amino acids at either the C or N terminus of the AMP. This post-translational processing generates a large diversity of alyteserin peptide variants (alyteserin-PVs).

Alyteserin AMPs show variable ability to inhibit *Bd* in vitro

To investigate whether the AMPs from *A. obstetricans* represent an effective defense against *Bd*, we performed in vitro *Bd* growth inhibition assays against a panel of known AMPs in the species. This included all seven previously described alyteserin 1 and alyteserin 2 AMPs described previously[32] (two of which were not found in our study system) and alyteserin 2 Mb (which we found in *A. obstetricans* within this study). Despite their reported universal efficacy against bacteria[32,41], they showed variable ability to inhibit the growth of *Bd* in vitro (Supplementary Table 2). Only alyteserin 1a (half-maximal effective concentration (EC_{50}) = 8.47 µmol), alyteserin 1b (EC_{50} = 41.03 µmol), alyteserin 2c (EC_{50} = 37.14 µmol) and alyteserin 2 Mb (EC_{50} = 7.53 µmol) were found to be inhibitory against *Bd*.

https://doi.org/10.1038/s41589-026-02254-6

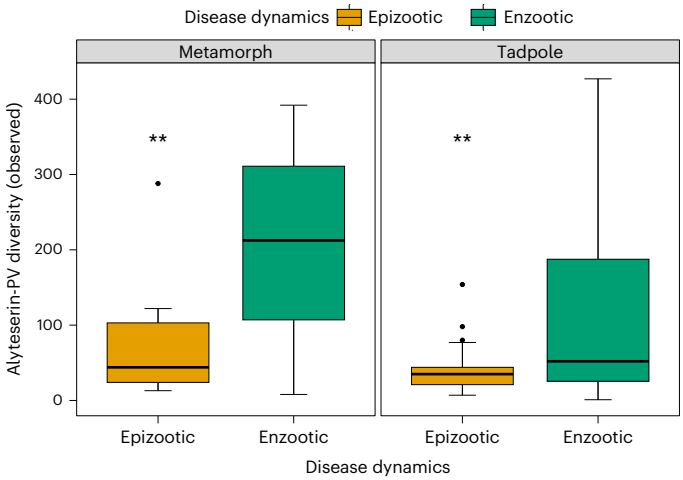


Fig. 4 | Epizootic disease dynamics are associated with lower alyteserin-PV diversity. Box plot showing that *A. obstetricans* at the epizootic Lac d'Arlet population has a significantly lower alyteserin-PV diversity at both postmetamorphic (Ibón de Acherito, $n = 40$; Lac d'Arlet, $n = 9$; Lac d'Lhurs, $n = 37$; Puits d'Arious, $n = 37$) and larval (Ibón de Acherito, $n = 37$; Lac d'Arlet, $n = 43$; Lac d'Lhurs, $n = 40$; Puits d'Arious, $n = 34$) life stages than in the enzootic populations. Box plots show the median (center), 25th and 75th percentiles (box limits) and 1.5× the interquartile range (whiskers). All individuals represent biological replicates. Significance was determined using a two-sided Wilcoxon rank-sum test for larval ($W = 3{,}095$, $P = 0.004$) and postmetamorphic ($W = 208$, $P = 0.003$) life stages. Box plots show the median (center), 25th and 75th percentiles (box limits) and 1.5× the interquartile range (whiskers). Significance is denoted by $^{*}P < 0.05$, $^{**}P < 0.01$ and $^{***}P < 0.001$.

We then carried out a preliminary investigation into elucidating the mode of action of alyteserin AMPs against *Bd*. It is generally thought that AMPs from frog skin secretions exert their antibacterial activity by disruption of the bacterial membrane[43]. Both the alyteserins and the temporins contain amphipathic sequences that adopt α-helical structures in membranes and in membrane-mimicking environments, leading to cell lysis; furthermore, changes in the sequences that promote helicity and membrane interactions enhance antibacterial activity[44]. The activity of temporin family peptides against *Bd* has also been hypothesized to depend on membrane disruption. An all-D-analog of temporin A was found to adopt an α-helical conformation in trifluoroethanol (TFE) and had enhanced potency against *Bd*[16], suggesting a membrane disruption rather than a receptor-binding mode of action. As similar structure–activity studies were not previously carried out with the alyteserins, we synthesized two of the most potent analogs (alyteserin 1a and alyteserin 2c) and a scrambled analog (scr-alyteserin 2c) as a control to study their conformational properties (Supplementary Documents 1 and 2). Circular dichroism (CD) measurements in both TFE and in 10 mM SDS showed that alyteserin 1a adopted a predominantly α-helical conformation in both solvents. This was less pronounced for alyteserin 2c and scr-alyteserin 2c had little or no secondary structure (Supplementary Document 3). To further probe the binding localization of the alyteserin informing on potential mode of action, we stained killed *Bd*-GPL isolate IA042 against Cy3-labeled versions of Alyteserin 1a, alyteserin 2c and scr-alyteserin 2c (Supplementary Document 1). Contrary to expectations, both alyteserin 1a and alyteserin 2c appeared to stain intracellular structures of *Bd* inside both the mature zoosporangia and the encysting zoospores (Fig. 3). The control scrambled alyteserin 2c did not expose such staining patterns, as only random fluorescent puncta were observed across the imaging areas. As these puncta did not seem to consistently locate with a killed chytrids, such signals were considered as background signal (Fig. 3). Collectively, the exclusive intracellular localization of the active versions of alyteserin suggests an intracellular inhibition mode of action involving either a specific partner or an interaction with intracellular membranes (Fig. 3).

Reduced peptide diversity is associated with epizootic disease dynamics

We found that the alpha diversity of alyteserin-PVs was significantly lower in the epizootic population compared to the three enzootic populations (Fig. 4) across both larval (Wilcoxon test: $W = 3095$, $P = 0.004$) and postmetamorphic (Wilcoxon test: $W = 208$, $P = 0.003$) life stages. We then investigated whether these trends in alyteserin-PV diversity were associated with developmental differences in the restructuring of the skin-secreted peptidome through metamorphosis.

Maturity of AMP defenses is not intrinsically linked to metamorphosis

To characterize the changes in the skin-secreted AMP defenses through metamorphosis, we performed differential abundance analysis of the alyteserin-PVs between larval and postmetamorphic life stages within each population. We found that the numbers of differentially abundant peptides ($\log_2$ fold change > 1, Hochberg corrected P value < 0.05) varied substantially between populations (Fig. 5a). There were a total of 121 unique alyteserin-PVs with significantly increased abundance in postmetamorphic individuals at Puits d'Arious ($n = 98$) and Lac de Lhurs ($n = 58$). However, there were no differentially abundant peptides between life stages at either Lac d'Arlet or Ibon de Acherito. We then performed a hierarchical, complete-linkage clustering analysis on these differentially abundance peptides (Fig. 5b). Surprisingly, the two clusters identified by the basal node of this analysis did not clearly separate larval and postmetamorphic life stages. Instead, each of these two clusters comprised a mixture of both life stages. The first cluster comprised mostly the postmetamorphic life stage (123/184 individuals) and was characterized by a higher compositional abundance of the differentially abundant secreted peptides. The second cluster comprised mostly the larval life stage (93/123 individuals) and was characterized by a lower compositional abundance of the differentially abundant secreted peptides. We assigned these clusters as 'complex AMP phenotype' and 'simple AMP phenotype', respectively.

We then performed a principal component analysis (PCA) to investigate the relative contributions of life stage, cluster membership and *Bd* infection status on the composition of these differentially abundant peptides (Fig. 5c). We found that cluster membership was a substantially stronger predictor of secreted peptidome composition than life stage or *Bd* infection (PERMANOVA: cluster membership, $R^2 = 0.24$, $P < 0.001$; life stage, $R^2 = 0.02$, $P < 0.001$; *Bd* infection status, $R^2 = 0.01$, $P < 0.01$; cluster membership × life stage, $R^2 = 0.01$, $P < 0.001$).

Immature AMP phenotypes are deficient in anti-*Bd* AMPs

The proportion of postmetamorphic individuals with a simple AMP phenotype was significantly higher (Fisher's exact test: $P = 0.007$) in the epizootic population than the enzootic populations (Fig. 6a). We then wanted to test whether the lower alpha diversity of alyteserin-PVs in postmetamorphic animals at Lac d'Arlet (Fig. 4) was explained by this over-representation of simple AMP phenotypes.

We fitted a mixed-effect model of observed peptide diversity with cluster membership as an interacting effect, bodyweight and life stage as fixed effects and site as a random effect. We found that cluster membership was a strong predictor of observed peptide diversity (GlmmTMB: estimate = −152.68, s.e. = 11.85, $z = -12.89$, $P < 0.001$). Bodyweight (GlmmTMB: Est = 47.44, s.e. = 27.17, $z = 1.75$, $P > 0.05$) and life stage (GlmmTMB: Est = −32.08, s.e. = 17.69, $z = -1.81$, $P > 0.05$) were marginally nonsignificant. Across both life stages, complex AMP phenotypes possessed significantly higher alyteserin-PV alpha diversity than simple AMP phenotypes (Fig. 6b). Lastly, postmetamorphic animals with simple AMP phenotypes produced significantly smaller (bodyweight-normalized) quantities of *Bd*-inhibitory alyteserin 1a (Wilcoxon test: $Z = 3.56$, $P < 0.001$), alyteserin

https://doi.org/10.1038/s41589-026-02254-6

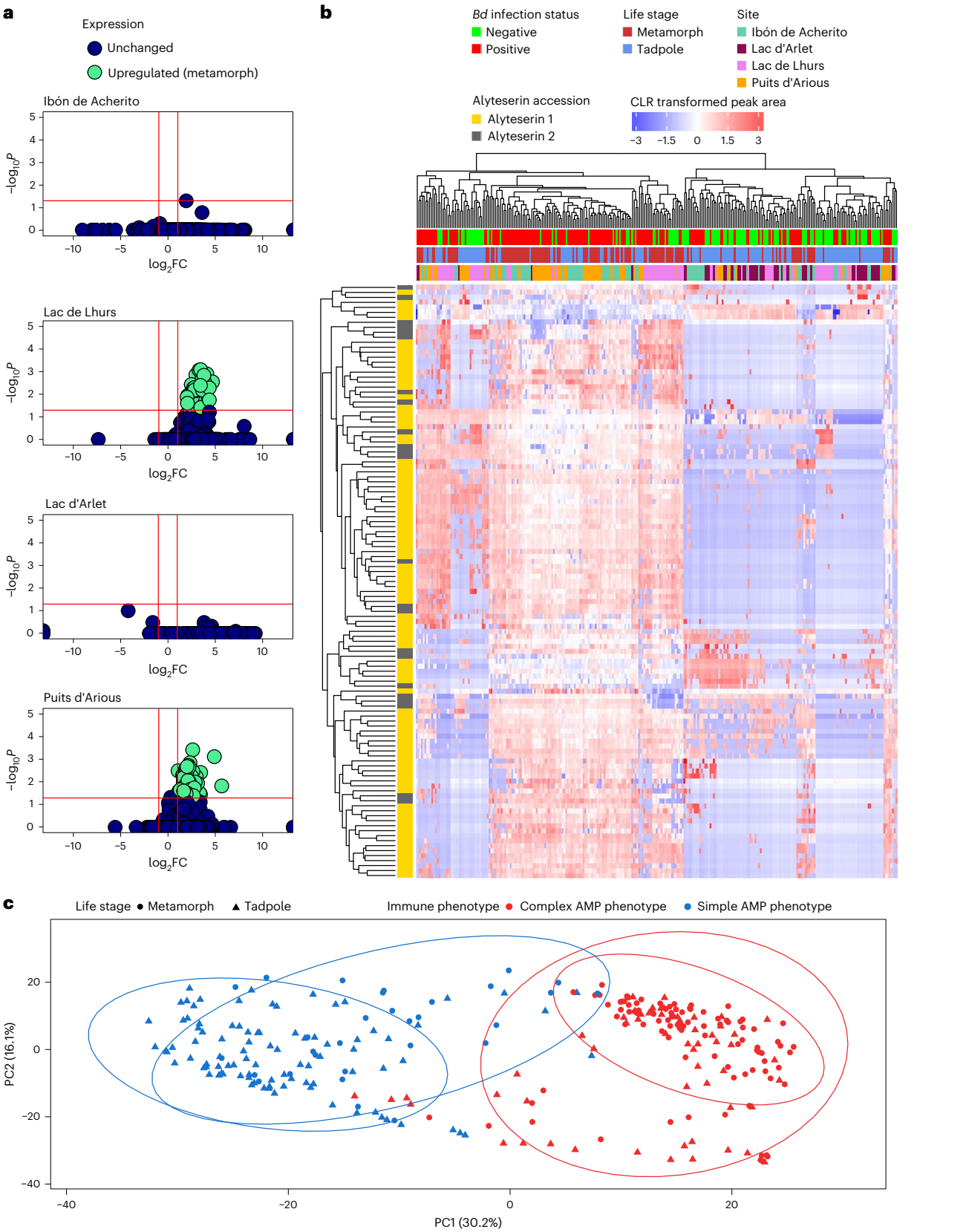


Fig. 5 | AMP maturation across four populations of *A. obstetricans*. **a**, Differential abundance analysis of Alyteserin-aligned peptides between life stages in each population. Significance was determined using a Wilcoxon rank-sum test at $P < 0.05$, with Hochberg correction for multiple comparisons. FC, fold change. **b**, Heat map showing that the clustering of differentially abundant peptides does not partition by life stage. Instead, there is a cluster with a high relative abundance of AMPs (mature AMP phenotype; left) and a cluster with a low relative abundance of AMPs (immature AMP phenotype; right). **c**, PCA showing that cluster membership, not life stage, is the strongest predictor of secreted peptide composition. All individuals represent biological replicates.

https://doi.org/10.1038/s41589-026-02254-6

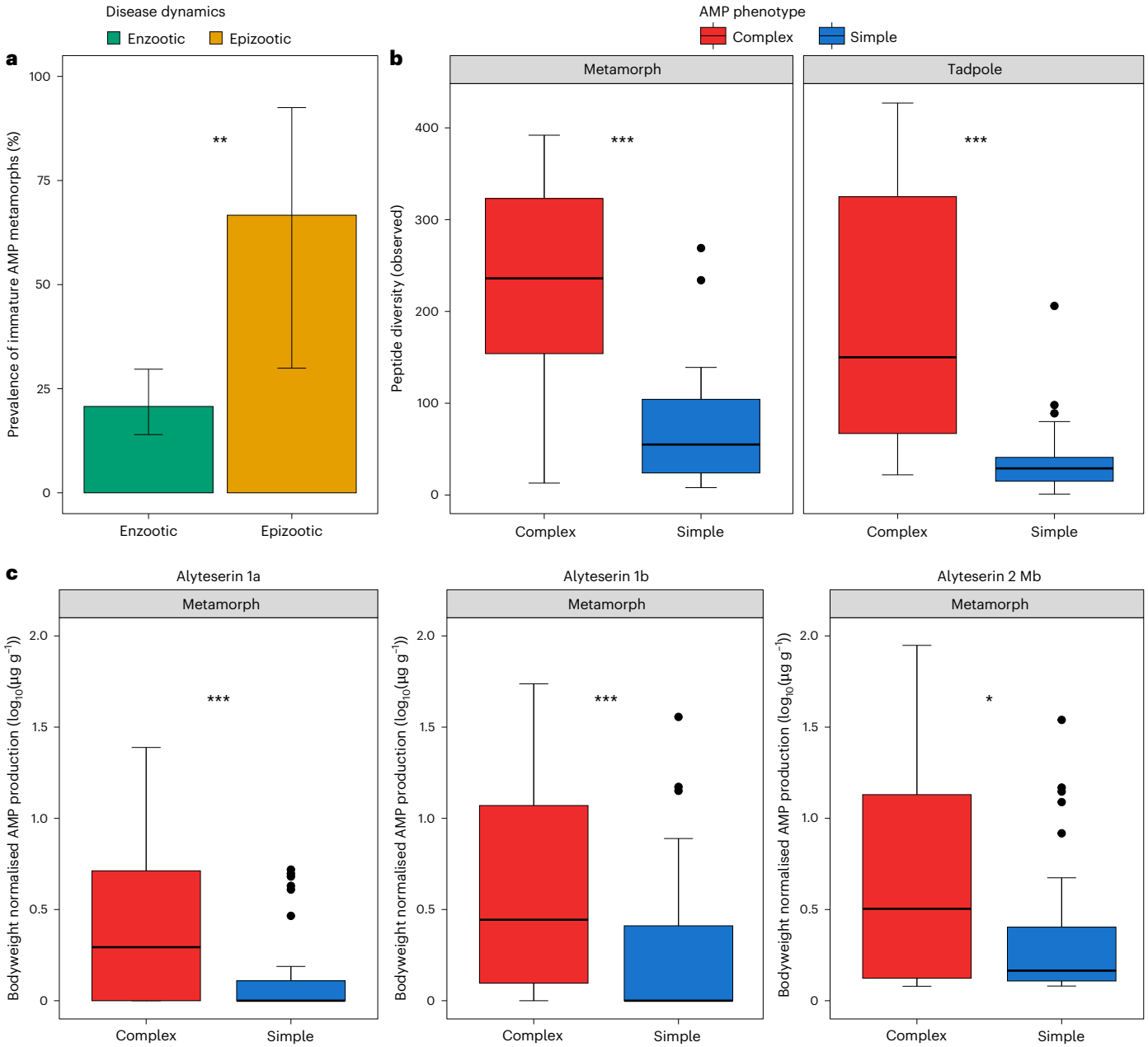


Fig. 6 | Timing of immune maturation is associated with *Bd* disease dynamics. **a**, Bar chart showing a significantly higher relative abundance of metamorphs with an immature AMP phenotype at the epizootic Lac d'Arlet ($N = 9$) population compared to the three enzootic populations ($N = 114$). Significance was determined using a Fisher's exact test ($P = 0.007$). **b**, Box plot showing the significantly higher diversity of alyteserin-aligned peptides in animals with a mature (cluster 1) AMP phenotype (larvae, $n = 61$; postmetamorphic, $n = 93$) than immature (cluster 2) AMP phenotypes (larvae, $n = 93$; postmetamorphic, $n = 30$) across both life stages. Significance was determined using a two-sided Wilcoxon rank-sum test for larval ($W = 5186$, $P < 0.001$) and postmetamorphic ($W = 2502$, $P < 0.001$) life stages. **c**, Box plots showing the significantly higher bodyweight-normalized quantity of the three anti-*Bd* Alyteserins in recent metamorphs with a mature AMP phenotype ($n = 93$) than an immature AMP phenotype ($n = 30$). Significance was tested using an asymptotic Wilcoxon–Mann–Whitney test individually for alyteserin 1a ($Z = 3.56$, $P < 0.001$), alyteserin 1b ($Z = 3.36$, $P < 0.001$) and alyteserin 2 Mb ($Z = 2.46$, $P = 0.013$). All individuals represent biological replicates. Box plots show the median (center), 25th and 75th percentiles (box limits) and 1.5× the interquartile range (whiskers). Significance is denoted by $^*P < 0.05$, $^{**}P < 0.01$ and $^{***}P < 0.001$.

1b (Wilcoxon test: $Z = 3.36$, $P < 0.001$) and alyteserin 2 Mb (Wilcoxon test: $Z = 2.46$, $P = 0.013$) (Fig. 6c).

Discussion

This study challenges the paradigm of immune maturation being a fixed process through the ontogeny of organisms with a biphasic life history. This maturation process was presumed to be a transition from an immature ('simple') larval AMP phenotype to a mature ('complex') postmetamorphic AMP phenotype. We show that the timing of innate immune maturation relative to metamorphosis is associated with population-level disease dynamics in *A. obstetricans*. Animals that metamorphose before AMP immune maturity display a simple, low-diversity alyteserin-PV phenotype deficient in *Bd*-inhibitory AMPs. Study sites that have perennially declined following the emergence of *Bd* are characterized by a high prevalence of *A. obstetricans* manifesting this simple, low-diversity alyteserin-PV phenotype.

We show that the timing of immune maturation of amphibians is not intrinsically tied to metamorphosis. We further show that immune

maturation may occur before metamorphosis and metamorphosis may occur without immune maturation. However, little is known about the factors that determine this timing. Whilst we acknowledge that a genetic component of this variation is likely, larval development in amphibians is known to be a highly plastic process. A wide range of interacting ecological factors experienced at the larval stage such as temperature, larval density, the presence of predators and food availability can influence many host traits, including skin chemistry. Although we are unable to produce definitive evidence to support our hypothesis, we believe that the process of larval overwintering in *A. obstetricans* likely explains this variation in immune investment before metamorphosis. Rather unusually for amphibians, *A. obstetricans* tadpoles can either achieve metamorphosis within a single year or potentially overwinter for one or more years before metamorphosis[45]. Overwintering is more common in high-elevation populations of *A. obstetricans*, likely because of constraints on the annual period of activity by the lower temperatures in montane habitats. This lack of overwintering and the shorter annual activity periods may leave tadpoles with insufficient resources to invest in immune development; accordingly, they metamorphose without mature AMP defenses. Our results highlight the importance of studying both amphibian life stages to understand population-level disease dynamics.

Through the application of MS-based peptidomics, we revealed that the diversity of secreted peptides from amphibian skin is far higher than was previously appreciated[32]. We found that 45% of these peptides had significant alignment with six known alyteserin AMPs. Interestingly, much of this variation appears to be driven by post-translational modifications. This includes the characterization of both C-terminal acid and C-terminal amide analogs of all six Alyteserin AMPs in these populations, modifications known to be functionally important in membrane interactions with bacteria[46]. The remaining modifications were likely driven by hydrolysis of mature AMPs and variation in the cleavage sites of mature AMPs from their protein precursor.

This increased complexity of amphibian AMP phenotypes also has broad implications for the study of immunity and eco-evolutionary theory. The innate immune system has long been thought of as a primitive, blunt instrument comprising a limited number of broad-spectrum antimicrobial effectors. However, this assumption is increasingly recognized as being inaccurate[5,8]. We demonstrated that alyteserins show antimicrobial selectivity in their inhibitory activity and post-translational modifications are driving a vast diversification of the peptidome from the transcribed proteome. However, despite these insights, we are currently unable to assess whether skin AMPs represent an inducible or constitutive defense against *Bd*. While *Bd* infection was a poor predictor of the overall composition of alyteserin-PVs, further work under controlled, laboratory conditions will be needed to assess whether individual AMPs are modulated in response to *Bd* infection.

The implications for this increase in characterized peptide diversity are complex. Currently, our ability to characterize these complex biological mixtures far exceeds our ability to understand their function. Machine-learning tools are now available that aim to predict the conformation[47] or function[42] of peptides from amino acid sequence. However, the current tools come with three primary limitations with respect to this study system. Firstly, many of these tools treat antimicrobial activity as a binary response variable, which ignores the nuances of the antimicrobial selectivity of host AMPs. All six known alyteserin AMPs found within this study are reported to show inhibitory activity to bacteria[32] while only three of these peptides inhibit the growth of *Bd* in vitro. Secondly, the predicted tertiary structures and physiochemical characteristics derived from amino acid sequence are an integral part of predicting AMP activity (Supplementary Fig. 1). These properties are optimized for identifying AMPs that will interact with bacterial membranes, not the intracellular fungal inhibition demonstrated in this study. Further work is needed to understand the physiochemical properties of AMPs that inhibit fungi and how fungal pathogens are targeted by AMPs rather than the host's epithelial cells. The traditional models of AMP activity show that initial interactions take places by electrostatic attraction between cationic AMPs and negatively charged phospholipid head groups of bacteria[48]. However, the keratinized tissue in which *Bd* encysts is also negatively charged[49]. A greater understanding of the properties of the membranes of amphibian epithelial cells and *Bd* will greatly improve our ability to perform in silico screenings of putative AMPs from large peptidomic datasets. Lastly, these tools assume 'independence of action' of AMPs. Although this is currently an unreasonable expectation of machine-learning tools, AMPs are known to interact with pathogens synergistically[33,34] and 'noninhibitory' AMPs may act synergistically with other peptides to inhibit pathogen growth. However, with the rapid developments in this field, our ability to generate in silico predictions is constantly improving and future studies will be able to start to overcome these barriers.

The low alyteserin-PV diversity of the epizootic Lac d'Arlet population relative to the enzootic populations mirrors previous work with skin microbiomes in these populations[2,4]. The skin microbiome acts as extended immunity through the inhibition of *Bd* growth as a function of the production of anti-*Bd* metabolites[17]. These mucosal microbial communities are shaped and regulated through host AMP production[50]. However, in many epithelial systems, there is extensive bidirectional crosstalk between the host's innate immunity and the microbiome[51]. This can include host immune priming modulated by the secretome of the skin microbiome when confronted by pathogens[52]. Future work should address these parallel observations through an integrative 'holobiont' approach to skin mucosal immunity.

Our results show that even intrinsically susceptible amphibian species can possess the tools that allow populations to recover following a severe *Bd* epizootic outbreak. In this study, we show that the timing of innate immune maturation relative to metamorphosis is associated with population-level disease dynamics in *A. obstetricans*. Animals that metamorphose before AMP immune maturity display a low-diversity AMP phenotype deficient in anti-*Bd* AMPs. A high incidence of these postmetamorphic animals with immature AMPs is associated with epizootic disease dynamics and population decline. These observed differences in host immune phenotype development are likely a crucial mechanism for establishing stable host–pathogen coexistence. As these immune phenotypes and biphasic history are highly generalizable across the class Amphibia, our results suggest that the timing of innate immune maturation may underlie the observed rebound in other *Bd*-susceptible amphibian species.

Online content

Any methods, additional references, Nature Portfolio reporting summaries, source data, extended data, supplementary information, acknowledgements, peer review information; details of author contributions and competing interests; and statements of data and code availability are available at https://doi.org/10.1038/s41589-026-02254-6.

References

1. Anderson, R. M. & May, R. M. The invasion, persistence and spread of infectious diseases within animal and plant communities. *Philos. Trans. R. Soc. Lond. B Biol. Sci.* **314**, 533–570 (1986).
2. Bates, K. A. et al. Amphibian chytridiomycosis outbreak dynamics are linked with host skin bacterial community structure. *Nat. Commun.* **9**, 693 (2018).
3. Briggs, C. J., Knapp, R. A. & Vredenburg, V. T. Enzootic and epizootic dynamics of the chytrid fungal pathogen of amphibians. *Proc. Natl Acad. Sci. USA* **107**, 9695–9700 (2010).
4. Bates, K. A. et al. Microbiome function predicts amphibian chytridiomycosis disease dynamics. *Microbiome* **10**, 44 (2022).
5. Lazzaro, B. P., Zasloff, M. & Rolff, J. Antimicrobial peptides: application informed by evolution. *Science* **368**, eaau5480 (2020).

6. Zhang, L. J. & Gallo, R. L. Antimicrobial peptides. *Curr. Biol.* **26**, R14–R19 (2016).
7. Beutler, B. Innate immunity: an overview. *Mol. Immunol.* **40**, 845–859 (2004).
8. Hanson, M. A., Kondo, S. & Lemaitre, B. *Drosophila* immunity: the *Drosocin* gene encodes two host defence peptides with pathogen-specific roles. *Proc. Biol. Sci.* **289**, 20220773 (2022).
9. Fisher, M. C. et al. Emerging fungal threats to animal, plant and ecosystem health. *Nature* **484**, 186–194 (2012).
10. Scheele, B. C. et al. Amphibian fungal panzootic causes catastrophic and ongoing loss of biodiversity. *Science* **363**, 1459–1463 (2019).
11. Voyles, J. et al. Pathogenesis of chytridiomycosis, a cause of catastrophic amphibian declines. *Science* **326**, 582–585 (2009).
12. Alonso, A., Monroy, S., Bosch, J., Pérez, J. & Boyero, L. Amphibian loss alters periphyton structure and invertebrate growth in montane streams. *J. Anim. Ecol.* **91**, 2329–2337 (2022).
13. Whiles, M. R. et al. The effects of amphibian population declines on the structure and function of neotropical stream ecosystems. *Front. Ecol. Environ.* **4**, 27–34 (2006).
14. Zipkin, E. F., DiRenzo, G. V., Ray, J. M., Rossman, S. & Lips, K. R. Tropical snake diversity collapses after widespread amphibian loss. *Science* **367**, 814–816 (2020).
15. Rosa, G. M. et al. Seasonality of host immunity in a tropical disease system. *Ecosphere* **13**, e4158 (2022).
16. Rollins-Smith, L. A. The role of amphibian antimicrobial peptides in protection of amphibians from pathogens linked to global amphibian declines. *Biochim. Biophys. Acta* **1788**, 1593–1599 (2009).
17. Harris, R. N. et al. Skin microbes on frogs prevent morbidity and mortality caused by a lethal skin fungus. *ISME J.* **3**, 818–824 (2009).
18. Woodhams, D. C., Voyles, J., Lips, K. R., Carey, C. & Rollins-Smith, L. A. Predicted disease susceptibility in a Panamanian amphibian assemblage based on skin peptide defenses. *J. Wildl. Dis.* **42**, 207–218 (2006).
19. Rollins-Smith, L. A. et al. Activities of temporin family peptides against the chytrid fungus (*Batrachochytrium dendrobatidis*) associated with global amphibian declines. *Antimicrob. Agents Chemother.* **47**, 1157–1160 (2003).
20. Humphries, J. E. et al. Do immune system changes at metamorphosis predict vulnerability to chytridiomycosis? An update. *Dev. Comp. Immunol.* **136**, 104510 (2022).
21. Longcore, J. E., Pessier, A. P. & Nichols, D. K. *Batrachochytrium dendrobatidis* gen. et sp. nov., a chytrid pathogenic to amphibians. *Mycologia* **91**, 219–227 (1999).
22. Marantelli, G., Berger, L., Speare, R. & Keegan, L. Distribution of the amphibian chytrid Batrachochytrium dendrobatidis and keratin during tadpole development. *Pac. Conserv. Biol.* **10**, 173–179 (2004).
23. Garner, T. W. J. et al. Life history tradeoffs influence mortality associated with the amphibian pathogen *Batrachochytrium dendrobatidis*. *Oikos* **118**, 783–791 (2009).
24. Rollins-Smith, L. A. Metamorphosis and the amphibian immune system. *Immunol. Rev.* **166**, 221–230 (1998).
25. Calhoun, D. M. et al. Role of antimicrobial peptides in amphibian defense against trematode infection. *Ecohealth* **13**, 383–391 (2016).
26. Robert, J. & Ohta, Y. Comparative and developmental study of the immune system in *Xenopus*. *Dev. Dyn.* **238**, 1249–1270 (2009).
27. Schadich, E., Cole, A. L. J., Squire, M. & Mason, D. Skin peptides of different life stages of Ewing's tree frog. *J. Exp. Zool. A Ecol. Genet. Physiol.* **313A**, 532–537 (2010).
28. Holden, W. M., Reinert, L. K., Hanlon, S. M., Parris, M. J. & Rollins-Smith, L. A. Development of antimicrobial peptide defenses of southern leopard frogs, Rana sphenocephala, against the pathogenic chytrid fungus, *Batrachochytrium dendrobatidis*. *Dev. Comp. Immunol.* **48**, 65–75 (2015).
29. Tobler, U. & Schmidt, B. R. Within- and among-population variation in chytridiomycosis-induced mortality in the toad *Alytes obstetricans*. *PLoS ONE* **5**, e10927 (2010).
30. Rosa, G. M. et al. Evidence of chytrid-mediated population declines in common midwife toad in Serra da Estrela, Portugal. *Anim. Conserv.* **16**, 306–315 (2013).
31. Bosch, J., Martínez-Solano, I. & García-París, M. Evidence of a chytrid fungus infection involved in the decline of the common midwife toad (*Alytes obstetricans*) in protected areas of central Spain. *Biol. Conserv.* **97**, 331–337 (2001).
32. Conlon, J. M. et al. The alyteserins: two families of antimicrobial peptides from the skin secretions of the midwife toad *Alytes obstetricans* (Alytidae). *Peptides* **30**, 1069–1073 (2009).
33. Ferguson, P. M. et al. Temporin B forms hetero-oligomers with temporin L, modifies its membrane activity, and increases the cooperativity of its antibacterial pharmacodynamic profile. *Biochemistry* **61**, 1029–1040 (2022).
34. Bechinger, B., Juhl, D. W., Glattard, E. & Aisenbrey, C. Revealing the mechanisms of synergistic action of two magainin antimicrobial peptides. *Front. Med. Technol.* **2**, 615494 (2020).
35. Aebersold, R. & Mann, M. Mass spectrometry-based proteomics. *Nature* **422**, 198–207 (2003).
36. Aebersold, R. & Mann, M. Mass-spectrometric exploration of proteome structure and function. *Nature* **537**, 347–355 (2016).
37. Savaryn, J. P., Catherman, A. D., Thomas, P. M., Abecassis, M. M. & Kelleher, N. L. The emergence of top-down proteomics in clinical research. *Genome Med.* **5**, 53 (2013).
38. Macklin, A., Khan, S. & Kislinger, T. Recent advances in mass spectrometry based clinical proteomics: applications to cancer research. *Clin. Proteomics* **17**, 17 (2020).
39. Wang, G., Li, X. & Wang, Z. APD3: the antimicrobial peptide database as a tool for research and education. *Nucleic Acids Res.* **44**, D1087–D1093 (2016).
40. Tran, N. H., Zhang, X., Xin, L., Shan, B. & Li, M. De novo peptide sequencing by deep learning. *Proc. Natl Acad. Sci. USA* **114**, 8247–8252 (2017).
41. König, E. et al. Antimicrobial peptides and alytesin are co-secreted from the venom of the midwife toad, *Alytes maurus* (Alytidae, Anura): implications for the evolution of frog skin defensive secretions. *Toxicon* **60**, 967–981 (2012).
42. Santos-Júnior, C. D., Pan, S., Zhao, X. M. & Coelho, L. P. MACREL: antimicrobial peptide screening in genomes and metagenomes. *PeerJ* **8**, e10555 (2020).
43. Subasinghage, A. P., O'Flynn, D., Conlon, J. M. & Hewage, C. M. Conformational and membrane interaction studies of the antimicrobial peptide alyteserin-1c and its analogue [E4K] alyteserin-1c. *Biochim. Biophys. Acta* **1808**, 1975–1984 (2011).
44. Manzo, G. et al. Minor sequence modifications in temporin B cause drastic changes in antibacterial potency and selectivity by fundamentally altering membrane activity. *Sci. Rep.* **9**, 1385 (2019).
45. Michaels, C. J., Bosch, J., Jervis, P. A., Márquez, R. & Rosa, G. M. *Midwife Toads—The Genus Alytes: History, Ecology, Systematics, Captive Breeding*. (Edition Chimaira, 2023).
46. Chaudhary, A., Prasad, A., Martin, L. L. & Panwar, A. S. The impact of C-terminal amidation on antimicrobial peptide behavior: insights from molecular dynamics simulations approach. In *Proc. International Conference on Mathematical Methods and Models in Biosciences* (Biomath, 2023).
47. Jumper, J. et al. Highly accurate protein structure prediction with AlphaFold. *Nature* **596**, 583–589 (2021).
48. Sato, H. & Feix, J. B. Peptide–membrane interactions and mechanisms of membrane destruction by amphipathic α-helical antimicrobial peptides. *Biochim. Biophys. Acta* **1758**, 1245–1256 (2006).

49. Bragulla, H. H. & Homberger, D. G. Structure and functions of keratin proteins in simple, stratified, keratinized and cornified epithelia. *J. Anat.* **214**, 516–559 (2009).
50. Franzenburg, S. et al. Distinct antimicrobial peptide expression determines host species-specific bacterial associations. *Proc. Natl Acad. Sci. USA* **110**, E3730–E3738 (2013).
51. Zheng, D., Liwinski, T. & Elinav, E. Interaction between microbiota and immunity in health and disease. *Cell Res.* **30**, 492–506 (2020).
52. Baquer, F. et al. Skin microbiota secretomes modulate cutaneous innate immunity against *Borrelia burgdorferi* s.s. *Sci. Rep.* **13**, 16393 (2023).

Publisher's note Springer Nature remains neutral with regard to jurisdictional claims in published maps and institutional affiliations.

Open Access This article is licensed under a Creative Commons Attribution 4.0 International License, which permits use, sharing, adaptation, distribution and reproduction in any medium or format, as long as you give appropriate credit to the original author(s) and the source, provide a link to the Creative Commons licence, and indicate if changes were made. The images or other third party material in this article are included in the article's Creative Commons licence, unless indicated otherwise in a credit line to the material. If material is not included in the article's Creative Commons licence and your intended use is not permitted by statutory regulation or exceeds the permitted use, you will need to obtain permission directly from the copyright holder. To view a copy of this licence, visit http://creativecommons.org/licenses/by/4.0/.

© The Author(s) 2026

[1]Institute of Zoology, Zoological Society of London, London, UK. [2]MRC Centre for Global Infectious Disease Analysis, School of Public Health, Imperial College, London, UK. [3]Department of Chemistry, UCL, London, UK. [4]IMIB Biodiversity Research Institute (CSIC-Oviedo University-Principality of Asturias), Mieres, Spain. [5]Centre for Ecology, Evolution and Environmental Changes (cE3c) and Global Change and Sustainability Institute (CHANGE), Faculdade de Ciências da Universidade de Lisboa, Lisbon, Portugal. [6]Blizard Institute, The Faculty of Medicine and Dentistry, Queen Mary University of London, London, UK. [7]Department of Microbiology and Immunology, McGill University, Montreal, Québec, Canada. [8]Infectious Diseases and Immunity in Global Heath Program, Research Institute of the McGill University Health Centre, Montreal, Québec, Canada. [9]Department of Plant and Environmental Sciences, University of Copenhagen, Frederiksberg, Denmark. [10]Living Systems Institute, University of Exeter, Exeter, UK. [11]Laboratory of Virology, Wageningen University and Research, Wageningen, The Netherlands. [12]Zoological Society of London, London, UK. [13]Centre for Biomolecular Spectroscopy and Randall Division of Cell and Molecular Biophysics, King's College London, New Hunt's House, London, UK. [14]Centre for Ecology and Conservation, University of Exeter, Penryn, UK. [15]Radboud University Medical Centre, Department of Medical Microbiology, Nijmegen, The Netherlands. [16]School of Biosciences, University of Birmingham, Birmingham, UK. [17]Unit for Environmental Sciences and Management, Northwest University, Private Bag X6001, Potchefstroom, South Africa. ✉e-mail: Trent.Garner@ioz.ac.uk; matthew.fisher@imperial.ac.uk; a.b.tabor@ucl.ac.uk

Methods

Sample collection: field surveys

Field sampling took place between July 29 and August 6, 2019, and between August 3 and August 9, 2020. Animals were captured by hand or net and we sampled a maximum of 20 tadpoles and 20 postmetamorphic individuals per site (Supplementary Table 3). Recently metamorphosed individuals were found beneath cover objects bordering the lakes and any observed mortalities were recorded. These postmetamorphic animals only congregate near water for a few weeks before dispersing into strictly terrestrial habitats, which limits demographic structuring of the animals sampled[45]. Tadpoles had their mouthparts swabbed with an MW100 cotton-tipped swab (Medical Wire and Equipment) and postmetamorphic animals were swabbed according to a standard protocol; each specimen was swabbed by taking five strokes down the center of the underside, on each flank, the inside of the hind legs and bottom of the feet. Swabs were stored below 4 °C until DNA extraction. Peptide sampling was performed using a bath exposure of norepinephrine[53]. Briefly, each individual was exposed to a 200 µM bath of norepinephrine bitartrate (A0397, Merck) and high-performance LC (HPLC)-grade water (V270733, Merck) in a sterile Whirlpak bag (Nasco Sampling). After 15 min, the animal was removed from the Whirlpak and returned to its individual capture bag. The sample was then acidified by addition of 0.2 ml of trifluoroacetic acid (302031, Merck), returned from the field on ice and stored at −18 °C until purification for MS analysis. Each animal was contained in a new plastic bag and handled with a new pair of powder nitrile gloves to prevent cross-infection of individuals[54].

DNA extraction and *Bd* diagnostics

DNA from skin swabs was extracted in a PrepMan Ultra (Applied Biosystems). To assign the infection status and to quantify the disease burden of each individual, we performed *Bd*-ITS qPCR[55]. Extractions were diluted 1:10 before qPCR amplification, run in duplicate and considered to be positive if both wells amplified and were over 0.1 genomic equivalents (GE; where 1 GE is the quantity of genetic material present in a single zoospore). All samples were run against positive standards of 0.1, 1, 10 and 100 GE of *Bd*-GPL (isolate IA042) and negative control standards. Plates with a standard curve of $R^2 < 0.95$ were repeated.

Skin secretion sample prep

Skin secretion samples were concentrated and desalted through a C18 Sep-Pak cartridge (WAT020515, Waters) partial purification procedure[53]. Briefly, the Sep-Pak cartridge was primed with 2 ml of acetonitrile (270717, Merck), equilibrated with 2 ml of a 0.1% TFA wash solution before the sample was loaded. To maximize the yield, the wash and loading steps were repeated. Samples were then stored on the cartridges at 4 °C until analysis. Before MS analysis, the cartridge was washed with 4 ml of a 0.1% TFA wash solution before being eluted with 2 ml of 70% acetonitrile and 30% HPLC water with 0.1% TFA. The eluent was then frozen overnight at −80 °C and dried under vacuum using a Speedvac (Thermo-Savant).

LC–MS/MS analysis of field samples

Proteomic analysis of the semipurified amphibian skin secretions was performed using a Vanquisher LC system connected to a Q-Exactive plus quadrupole-orbitrap MS instrument (Thermo Scientific). Lyophilized skin secretions were resuspended in 100 µl of solvent (5% acetonitrile in water, 0.1% formic acid) and centrifuged for 5 min at 11,300*g*. Then, 20 µl of each sample was injected onto a Hypersil Gold column (150 mm × 2.1 mm, 3-µm particle size; 25002-1521300). The chromatographic peptides separation on this column was achieved using mobile phase A (water, 0.1% formic acid) and mobile phase B (acetonitrile, 0.1% formic acid). The 20-min gradient was as follows: 2 min with 5% B, before increasing to 99% B over the next 15 min, maintaining at 99% B for a further 3 min and then decreasing to 5% B within 6 s, maintained for 1.9 min to equilibrate the Hypersil C_{18} column. The flow rate was 0.2 ml min^{-1}. The column effluent was continuously directed to the heated electrospray ionization (HESI) source of the Q-Exactive MS instrument. The HESI probe was operated with sheath gas flow at 25, auxiliary gas flow at 5, spray voltage at 3.80, capillary temperature at 270 °C, S-lens radiofrequency level at 55 and auxiliary gas heater temperature at 50 °C. The Q-Exactive MS instrument was operated in a positive ion mode. MS data were acquired using a data-dependent acquisition mode and operated at 70,000 resolution (full width at half-maximum height definition). The top eight most abundant multiply charged ($z \geq 2$) ions in the 300–1,800 m/z range were selected for MS/MS, with dynamic exclusion enabled for 30 s. The automatic gain control for the Q-Exactive was set to 500,000 ions and the automatic gain control for the MS/MS in the ion trap was set at 8,000 ions. For MS/MS, the isolation width was set at 1.4 and the collision energy was 35%. MS/MS scans were acquired at a resolution of 17,500 at 200 m/z and the fixed first mass was set to 120 m/z. Three MS/MS microscans for each precursor were accumulated. Dynamic exclusion was enabled and selected ions were excluded for 20 s before they could be selected for another round of MS/MS.

Peptidomic reference libraries

To align the peptide sequences generated through MS, we used two references libraries. To identify known AMPs, we aligned all de novo sequences against the APD3 database[39].

To generate a full mucosal peptidome, we generated an RNA-seq reference library for both larval and postmetamorphic *A. obstetricans*. Skin samples (of three larval and three postmetamorphic *A. obstetricans*) up to 25 mg were collected and immediately stored in Trizol reagent. Samples were homogenized using a pestle in 1.5-ml tubes and total RNA was extracted using the standard Trizol RNA extraction protocol. Pelleted RNA was resuspended in 30 µl of RNase-free water. RNA integrity was quantified using an Agilent TapeStation 2100 bioanalyzer. Total RNA was quantified on a Qubit using the RNA high-sensitivity kit. Sample replicates were pooled equally to produce a single sample for library preparation. Samples were submitted to Novogene for mRNA library preparation (poly(A) enrichment) and paired-end 150-bp sequencing on an Illumina NovaSeq for 80 million reads per sample.

De novo assembly was performed using Trinity (version 2.8.5) using default parameters. Trimmomatic (version 0.39)[56] was used to quality trim reads and in silico normalization of reads was carried out. Resulting assemblies were quality assessed by examining the number of transcripts that appear full-length or nearly full-length. BLASTx (version 2.2.30), using the *Xenopis laevis* (XENLA_10.01_GCF_XBmodels.transcripts.fa) reference transcript set as a frog-specific comparison, was performed to assess the quality of the assemblies. It is sometimes the case that a single transcript will align to a single protein sequence with several discontinuous alignments (that is, a BLAST hit containing multiple hit-scoring segment pairs (HSPs)). Therefore, multiple HSPs were grouped per transcript and database hit and the alignment coverage based on grouped HSPs was also assessed. Bowtie2 (version 7.3.0)[57] was used to assess the alignment rate of RNA-seq reads back to the assembly. The two assemblies were then concatenated and underwent six-frame translation in EMBOSS sixpack[58] before being clustered into 95% similar sequences using CD-HIT[59].

Peptidomic pipeline

Downstream analysis of the MS data was conducted using PEAKs Studio (version 12.0; Bioinformatic Solutions). From 697,265 MS scans and 1,109,355 MS/MS scans, 1,073,825 peptide spectrum matches were identified using the DeepNovo algorithm[40] with the following parameters: no enzyme digestion, parent mass error tolerance of 10.0 ppm, fragment mass error tolerance of 0.02 Da and a maximum of three post-translational modifications per peptide. We then performed a two-round search of de novo sequences with a quality score > 70 against APD3 and then our transcriptome-derived *A. obstetricans* peptide library with an identification threshold of $-\log P > 20$. Lastly,

high-quality unaligned sequences were assembled into de novo peptide features. Label-free quantification using PEAKs Q (version 12.0; Bioinformatic Solutions) was used to quantify the expression levels of the peptides in each sample using the following parameters: retention time, 4–22 min; peptide quality, ≥5; peptide average area, $\geq 1 \times 10^6$; peptide charge, 1–5; protein significance, ≥20; fold change, ≥1.

AMP quantification

Relative quantification of AMPs was achieved through generating a standard curve using synthetic peptides supplied by Cambridge Research Biochemicals. Standards were made up at concentrations of 100 µM, 50 µM, 25 µM and 12.5 µM in 5% acetonitrile and 95% water with 0.1% formic acid using the same LC–MS method used for the amphibian secretion samples. Peak areas of the standards were measured using Xcalibur Qual browser (version 2.2; Thermo Scientific). All standard curves had an $R^2 > 0.95$.

In vitro *Bd* inhibition assays

Growth inhibition assays were conducted by challenging *Bd*-GPL343 with a dilution series (six replicates of 100 µM, 50 µM, 25 µM, 12.5 µM, 6.25 µM, 3.125 µM and 1.60 µM) of each AMP in a FLUOstar Omega optical density plate reader (BMG Labtech). The experimental set up included a positive control (50 µl of *Bd* and 50 µl of sterile water), negative control (50 µl of heat-killed *Bd* and 50 µl of sterile water) and blanks (50 µl of mTGHL medium and water)[60]. Blank-compensated optical density readings were taken daily and each well examined with a Leica inverted microscope to check for contamination. Contaminated wells were removed from the experiment. Readings on each plate were taken until the growth rate of the positive control had reached a plateau. Growth was measured as a percentage of the mean growth of the positive control wells on the day growth reached a plateau. Best fit log–log models were determined and fitted using R package DRC[61].

Confocal microscopy imaging of Cy3-labeled alyteserins with *Bd*

We challenged killed *Bd*-GPL isolate IA042 against Cy3-labeled alyteserin 1a, alyteserin 2c and scr-alyteserin 2c (Supplementary Document 1). Briefly, zoospores of *Bd*-GPLIA042 were isolated from a 3-day old culture by filtration of the mTGhL on a 10-µm filter. Then, 300 µl of the zoospore suspension were inoculated in Mattek petri dishes for 2 days at 17 °C. Young zoosporangia were then killed and blocked by replacing the medium with a solution of 0.5% sodium azide and 1× carbofree blocking solution (Vectorlabs) in 1× PBS and incubating at 37 °C for 15 min. As dead zoosporangia were used, the potential bias raised by the different biological activities of the alyteserins was alleviated and all zoosporangia could be stained with a similar concentration of alyteserins and fluorophores. Blocked zoosporangia were then incubated with 10 µM Cy3–alyteserins in 1× PBS overnight at 4 °C and counterstained with 10 µg ml^{-1} calcofluor white for 15 min. After two washes, zoosporangia were imaged on Zeiss LSM780 laser scanning confocal microscope accumulating *Z* stacks covering the entire organism with a ×63 objective.

Statistical methods

All statistical analyses were carried out in R (version 4.2.0)[62]. Proteomic data were handled in the R package phyloseq[63] and CLR data transformations were performed in the R package microbiome. Curve fitting of peptide inhibition data was performed in the R package DRC. All plots were generated using ggplot2 (ref. 64). The map of field sites was generated using the ESRI National Geographic (https://services.arcgisonline.com/ArcGIS/rest/services/NatGeo_World_Map/MapServer) and ESRI Gray (light; https://www.arcgis.com/home/item.html?id=8b3d38c0819547faa83f7b7aca80bd76) base layers in QGIS[65].

Reporting summary

Further information on research design is available in the Nature Portfolio Reporting Summary linked to this article.

Data availability

The MS proteomics data were deposited to the ProteomeXchange Consortium through the PRIDE partner repository with the dataset identifier PXD069814. All raw RNA reads were deposited to the European Bioinformatics Institute European Nucleotide Archive and National Center for Biotechnology Information Sequence Read Archive under project accession PRJEB95135. Skin transcriptome assemblies for the postmetamorphic and larval *A. obstetricans* were deposited to Zenodo (https://doi.org/10.5281/zenodo.17463202 and https://doi.org/10.5281/zenodo.17463248)[66,67]. All source data are available from DataDryad (https://doi.org/10.5061/dryad.k0p2ngfn6)[68]. Source data are provided with this paper.

Code availability

All R scripts are available from DataDryad (https://doi.org/10.5061/dryad.k0p2ngfn6)[68].

References

53. Conlon, J. M. & Sonnevend, A. Antimicrobial peptides in frog skin secretions. *Methods Mol. Biol.* **618**, 3–14 (2010).
54. Phillott, A. D. et al. Minimising exposure of amphibians to pathogens during field studies. *Dis. Aquat. Organ* **92**, 175–185 (2010).
55. Boyle, D. G., Boyle, D. B., Olsen, V., Morgan, J. A. & Hyatt, A. D. Rapid quantitative detection of chytridiomycosis (*Batrachochytrium dendrobatidis*) in amphibian samples using real-time Taqman PCR assay. *Dis. Aquat. Organ* **60**, 141–148 (2004).
56. Bolger, A. M., Lohse, M. & Usadel, B. Trimmomatic: a flexible trimmer for Illumina sequence data. *Bioinformatics* **30**, 2114–2120 (2014).
57. Langmead, B. & Salzberg, S. L. Fast gapped-read alignment with Bowtie 2. *Nat. Methods* **9**, 357–359 (2012).
58. Madeira, F. et al. Search and sequence analysis tools services from EMBL-EBI in 2022. *Nucleic Acids Res.* **50**, W276–w279 (2022).
59. Li, W. & Godzik, A. CD-HIT: a fast program for clustering and comparing large sets of protein or nucleotide sequences. *Bioinformatics* **22**, 1658–1659 (2006).
60. Voyles, J. et al. Shifts in disease dynamics in a tropical amphibian assemblage are not due to pathogen attenuation. *Science* **359**, 1517–1519 (2018).
61. Ritz, C., Strebig, J. C. & Ritz, M. C. Package 'DRC'. Version 3.0-1 (2016).
62. R Core Team. *R: A language and environment for statistical computing*. (R Foundation for Statistical Computing, 2013).
63. McMurdie, P. J. & Holmes, S. phyloseq: an R package for reproducible interactive analysis and graphics of microbiome census data. *PLoS ONE* **8**, e61217 (2013).
64. Wickham, H. ggplot2. *Wiley Interdiscip. Rev. Comput. Stat.* **3**, 180–185 (2011).
65. Dawson, N. et al. qgis/QGIS: 3.44.11. *Zenodo* https://doi.org/10.5281/zenodo.6139224 (2026).
66. Jervis, P. Alytes obstetricians de novo transcript assembly. *Zenodo* https://doi.org/10.5281/zenodo.17463202 (2025).
67. Jervis, P. OBS de novo transcript assembly. *Zenodo* https://doi.org/10.5281/zenodo.17463248 (2025).
68. Jervis, P. A., et al. Data from: Early maturation of host antimicrobial peptide defenses is associated with host-pathogen coexistence. *Data Dryad* https://doi.org/10.5061/dryad.k0p2ngfn6 (2026).

Acknowledgements

We would like to thank A. Bracken, T. Sewell, C. Wierzbicki, P. Ghosh, A. Loyau, D. Schmeller and H. Senetac for fieldwork support. S. Flower aided during sample prep. We would also like to thank the technical team at Bioinformatics Solutions (particularly K. Jurcic and D. Maloney) for assistance with running analyses in PEAKs Studio. We

would also like to thank J. Robert for his comments on earlier versions of the manuscript. We would like to acknowledge the Imaging facility of the Research Institute of the McGill University Health Center for the access to the confocal microscopes and expertise. The CD experiments described in this paper were carried out at the Optical Spectroscopy facility, Biomolecular Spectroscopy Center, King's College London. The instruments are funded by the Wellcome Trust and British Heart Foundation (202767/Z/16/Z and IG/16/2/32273). Ethical approval was given by the Zoological Society of London Institute of Zoology ethics committee (512-IoZ23). Field sampling in Spain was conducted under permits INAGA (500201/24/2019/00181) and INAGA (500201/24/2020/00544). Field sampling in France was conducted under permits issued by Parc National des Pyrenees. P.A.J. is funded by the Leverhulme Center for the Holobiont, Imperial College London and the Science and Solutions for a Changing Planet DTP, Grantham Institute, Imperial College London. This work was funded by Fundação para a Ciência e a Tecnologia through grant PTDC/BIA-CBI/2434/2021 awarded to G.M.R. and by the Spanish Ministry of Science, Innovation and Universities (MICIU) through grant PID2024-162285OB-I00 awarded to G.M.R. and J.B. GMR is also supported by MICIU through the Ramón y Cajal program (RYC2021-031914-I). A.M. is funded by the Engineering and Physical Sciences Research Council Doctoral Training Partnership EP/R513143/1 and by University College London Global Engagement Fund. T.W.J.G. is funded by NE/S000992/1. M.C.F. is a fellow of the Canadian Institute for Advanced Research Fungal Kingdoms program. He receives funding from Natural Environment Research Council NE/S000844/1 and Medical Research Council MR/R015600/1. MS instrumentation was purchased using Research Capital Investment Funding at University College London. K.A.B was funded by a Biotechnology and Biological Sciences Research Council New Investigator Award (BB/Z516661/1).

Author contributions

P.A.J., B.T., J.B., T.W.J.G., M.C.F. and A.B.T. led the study design. P.A.J., G.M.R., K.A.B., S.E. and E.J.S. carried out field sampling. P.A.J., G.M.R., K.A.B., K.K., A.M., T.D., D.F., K.H., F.L.M., C.J.M., T.J.M., C.N., C.S., E.J.S., T.T.B. and D.S. performed the lab work. P.A.J., K.K. and A.B.T. developed the peptidomic methods. P.A.J. and J.R. carried out bioinformatic processing. P.A.J., G.M.R., K.A.B. and X.A.H. carried out the statistical analysis. P.A.J., G.M.R., K.A.B., J.B., T.W.J.G., M.C.F. and A.B.T. produced the first manuscript draft. All authors contributed substantially to subsequent versions before first submission.

Competing interests

All authors declare no competing interests.

Additional information

Supplementary information The online version contains supplementary material available at https://doi.org/10.1038/s41589-026-02254-6.

Correspondence and requests for materials should be addressed to Trenton W. J. Garner, Matthew C. Fisher or Alethea B. Tabor.

Peer review information *Nature Chemical Biology* thanks the anonymous reviewers for their contribution to the peer review of this work.

Reprints and permissions information is available at www.nature.com/reprints.

nature portfolio

Corresponding author(s): Alethea B Tabor

Last updated by author(s): Mar 20, 2026

Reporting Summary

Nature Portfolio wishes to improve the reproducibility of the work that we publish. This form provides structure for consistency and transparency in reporting. For further information on Nature Portfolio policies, see our Editorial Policies and the Editorial Policy Checklist.

Statistics

For all statistical analyses, confirm that the following items are present in the figure legend, table legend, main text, or Methods section.

n/a	Confirmed
☐	☒ The exact sample size (*n*) for each experimental group/condition, given as a discrete number and unit of measurement
☐	☒ A statement on whether measurements were taken from distinct samples or whether the same sample was measured repeatedly
☐	☒ The statistical test(s) used AND whether they are one- or two-sided *Only common tests should be described solely by name; describe more complex techniques in the Methods section.*
☐	☒ A description of all covariates tested
☐	☒ A description of any assumptions or corrections, such as tests of normality and adjustment for multiple comparisons
☐	☒ A full description of the statistical parameters including central tendency (e.g. means) or other basic estimates (e.g. regression coefficient) AND variation (e.g. standard deviation) or associated estimates of uncertainty (e.g. confidence intervals)
☐	☒ For null hypothesis testing, the test statistic (e.g. *F*, *t*, *r*) with confidence intervals, effect sizes, degrees of freedom and *P* value noted *Give P values as exact values whenever suitable.*
☒	☐ For Bayesian analysis, information on the choice of priors and Markov chain Monte Carlo settings
☒	☐ For hierarchical and complex designs, identification of the appropriate level for tests and full reporting of outcomes
☒	☐ Estimates of effect sizes (e.g. Cohen's *d*, Pearson's *r*), indicating how they were calculated

Our web collection on statistics for biologists contains articles on many of the points above.

Software and code

Policy information about availability of computer code

Data collection: None

Data analysis: PEAKS Studio 12, R v 4.2.0, PEPFOLD 3

For manuscripts utilizing custom algorithms or software that are central to the research but not yet described in published literature, software must be made available to editors and reviewers. We strongly encourage code deposition in a community repository (e.g. GitHub). See the Nature Portfolio guidelines for submitting code & software for further information.

Data

Policy information about availability of data

All manuscripts must include a data availability statement. This statement should provide the following information, where applicable:

- Accession codes, unique identifiers, or web links for publicly available datasets
- A description of any restrictions on data availability
- For clinical datasets or third party data, please ensure that the statement adheres to our policy

The mass spectrometry proteomics data have been deposited to the ProteomeXchange Consortium (http://proteomecentral.proteomexchange.org) via the PRIDE partner repository with the dataset identifier PXD069814 (10.6019/PXD069814). All raw RNA reads have been deposited to EBI ENA and NCBI SRA under project accession PRJEB95135, Skin transcriptome assemblies for the post-metamorphic and larval A.obstetricans have been deposited to Zenodo at 10.5281/zenodo.17463202 and 10.5281/zenodo.17463248 respectively. All R scripts and processed peptide data are available at DOI: 10.5061/dryad.k0p2ngfn6.

Research involving human participants, their data, or biological material

Policy information about studies with human participants or human data. See also policy information about sex, gender (identity/presentation), and sexual orientation and race, ethnicity and racism.

Reporting on sex and gender	Not applicable- the research did not involve human participants
Reporting on race, ethnicity, or other socially relevant groupings	*Please specify the socially constructed or socially relevant categorization variable(s) used in your manuscript and explain why they were used. Please note that such variables should not be used as proxies for other socially constructed/relevant variables (for example, race or ethnicity should not be used as a proxy for socioeconomic status).* *Provide clear definitions of the relevant terms used, how they were provided (by the participants/respondents, the researchers, or third parties), and the method(s) used to classify people into the different categories (e.g. self-report, census or administrative data, social media data, etc.)* *Please provide details about how you controlled for confounding variables in your analyses.*
Population characteristics	*Describe the covariate-relevant population characteristics of the human research participants (e.g. age, genotypic information, past and current diagnosis and treatment categories). If you filled out the behavioural & social sciences study design questions and have nothing to add here, write "See above."*
Recruitment	*Describe how participants were recruited. Outline any potential self-selection bias or other biases that may be present and how these are likely to impact results.*
Ethics oversight	*Identify the organization(s) that approved the study protocol.*

Note that full information on the approval of the study protocol must also be provided in the manuscript.

Field-specific reporting

Please select the one below that is the best fit for your research. If you are not sure, read the appropriate sections before making your selection.

☐ Life sciences ☐ Behavioural & social sciences ☒ Ecological, evolutionary & environmental sciences

For a reference copy of the document with all sections, see nature.com/documents/nr-reporting-summary-flat.pdf

Ecological, evolutionary & environmental sciences study design

All studies must disclose on these points even when the disclosure is negative.

Study description	Epizootic outbreaks of invasive pathogens, such as the fungal pathogen Batrachochytnum dendrobatidis (Bd). are increasingly recognised as a global threat to biodiversity. However, not all susceptible host populations are equally Impacted by these disease outbreaks. While some populations persist despite intense infections and high mortality rates. others can transition to enzootic coexistence with the pathogen. Here, we use comparative peptidomics to identify differences in antimicrobial peptide (AMP) maturation in the Bd-susceptible Common midwife toads (Alytes obstetricans) through metamorphosis. Here we show that animals which metamorphose prior to AMP immune maturation display a low diversity AMP phenotype which is deficient on antl·Bd AMPs Where a high incidence of post-metamorphic animals occur with immature AMPs, populations are associated with epizootic disease dynamics. Conversely, populations associated with mature AMPs are stable following invasion of the pathogen. Our results show that even intrinsically susceptible amphibian species can possess the tools which allow populations to recover following a severe Bd epizootic.
Research sample	Skin swabs and skin mucosal samples from Alytes obstetricans
Sampling strategy	Field sampling took place between the 29th July and 6th August 2019, and the 3rd August and 9th August 2020. Animals were captured by hand or net, and we sampled a maximum of 20 tadpoles and 20 post-metamorphic individuals per site (Tab.S3). Recently metamorphosed individuals were found beneath cover objects bordering the lakes and any observed mortalities were recorded. These post metamorphic animals only congregate near water for a few weeks before dispersing into strictly terrestrial habitats, which limits demographic structuring of the animals sampled. Tadpoles had their mouthparts swabbed with a MW100 cotton-tipped swab (Medical Wire and Equipment Co Ltd, UK) and post-metamorphic animals were swabbed according to a standard protocol; each specimen was swabbed by taking five strokes down the centre of the underside, on each flank, the inside of the hind legs and bottom of the feet. Swabs were stored below 4°C until DNA extraction. Peptide sampling was performed using a bath-exposure of norepinephrine. Briefly, each individual was exposed to a 200µM bath of norepinephrine bitartrate (A0397, Merck, UK) and HPLC grade water (V270733, Merck, UK) in a sterile Whirlpak bag (Nasco sampling, US). After 15 minutes, the animal was removed from the Whirlpak and returned to its individual capture bag. The sample was then acidified by addition of 0.2 ml trifluoroacetoc acid (302031, Merck, UK), returned from the field on ice and stored at -18°C until purification for mass spectrometry analysis. Each animal was contained on a new plastic bag and handled with a new pair of powder-free nitrile gloves to prevent cross-infection of individuals.
Data collection	Proteomic analysis of the semi-purified amphibian skin secretions was performed using a Vanquisher LC system connected to a Q·Exactive plus quadrupole-orbitrap mass spectrometer (Thermo Scientific, USA). Lyophilised skin secretions were re-suspended in l00µL solvent (5% acetonitrile in water, 0.1 % formic acid), centrifuged for five minutes at 13,000 rpm. 20 µL of each sample was injected onto a Hypersil Gold, 150 mm x 2.1 mm, 3 µm particle size (P/N 25002-1521300) column. The chromatographic peptides

separation on this column was achieved using Mobile phase A (water, 0.1% formic acid) and Mobtle phase B (acetonitrile, 0.1% formic acid). Twenty minutes gradient was as follows:· After 2 min with 5% B, the proportion or B was raised to 99% B over the next 15 min, and maintained at 99% B for a further 3 min, after within 6 sec the proportion of B was changed to 5% for 1.9 min to equilibrate the Hypersil C18 column. The flow rate was 0.2 ml/min. The column effluent was continuously directed to the HESI source or the Q Exactive mass spectrometer. The HESI probe was operated with a sheath gas flow at 25, an auxiliary gas flow at 5, a spray voltage at 3.80, a capillary temperature at 270 °C, a S-lens RF level at 55, an auxiliary gas heater temperature was set at 50°C The Q Exactive mass spectrometer was operated in a positive ion mode. MS data was acquired using a data-dependent acquisition mode, and operated at 70,000 resolution (full width at half-maximum height, FWHM definition), and the top eight most abundant multiply charged (z ≥2) ions in the 300-1,800 m/z range were selected for MS/MS, with dynamic exclusion enabled 30 sec. The automatic gain control for the Q Exactive was set to 500,000 ions, and the automatic gain control for the MS/MS on the ion trap was set at 8,000 ions. For MS/MS, the Isolation width was set at 1.4 and the collision energy was 35%. MS/MS scans were acquired at a resolution of 17,500 at 200 m/z, the fixed first mass was set to 120 m/z. Three MS/MS microscans for each precursor were accumulated. Dynamic exclusion was enabled, and selected ions were excluded for 20 s before they could be selected for another round of MS/MS.

Timing and spatial scale	2 week sampling period, one sampling event per year over 2 years across 4 lakes in the Pyrenees
Data exclusions	N/A
Reproducibility	All animals which were characterised were included in the study. Raw data as well as processed data has been provided for the peptidomics
Randomization	All data was from field samples which were not divided into groups.
Blinding	Not applicable

Did the study involve field work? ☒ Yes ☐ No

Field work, collection and transport

Field conditions	Samples taken from four lakes in the Pyrenees
Location	Western Pyrenean Mountain range
Access & import/export	Field sampling in Spain was conducted under permits INAGA (ref. 500201/24/2019/00181) and INAGA (ref. 500201/24/2020/00544) Field sampling in France was conducted under permits issued by Pare National des Pyrenees.
Disturbance	Non-invasive sampling procedures. Access to field sites was via existing hiking trails

Reporting for specific materials, systems and methods

We require information from authors about some types of materials, experimental systems and methods used in many studies. Here, indicate whether each material, system or method listed is relevant to your study. If you are not sure if a list item applies to your research, read the appropriate section before selecting a response.

Materials & experimental systems

n/a	Involved in the study
☒	☐ Antibodies
☒	☐ Eukaryotic cell lines
☒	☐ Palaeontology and archaeology
☐	☒ Animals and other organisms
☒	☐ Clinical data
☒	☐ Dual use research of concern
☒	☐ Plants

Methods

n/a	Involved in the study
☒	☐ ChIP-seq
☒	☐ Flow cytometry
☒	☐ MRI-based neuroimaging

Animals and other research organisms

Policy information about studies involving animals; ARRIVE guidelines recommended for reporting animal research, and Sex and Gender in Research

Laboratory animals	6 Alytes obstetricans were used for developing RNAseq references

Wild animals	We sampled skin secretions from a total of 154 A. obstetricans tadpoles and 123 post-metamorphic individuals across the four survey sites. The amphibians were released unharmed after samphng the skin secretions
Reporting on sex	N/A
Field-collected samples	Skin secretion samples were acidified by addition of 0.2 ml trifluoroacetic acid (302031, Merck, UK), returned from the field on ice and stored at -18°C until purification for mass spectrometry analysis.
Ethics oversight	Ethical approval was given by the ZSL Institute of Zoology ethics committee (512-IoZ23)

Note that full information on the approval of the study protocol must also be provided in the manuscript.

Plants

Seed stocks	N/A
Novel plant genotypes	*Describe the methods by which all novel plant genotypes were produced. This includes those generated by transgenic approaches, gene editing, chemical/radiation-based mutagenesis and hybridization. For transgenic lines, describe the transformation method, the number of independent lines analyzed and the generation upon which experiments were performed. For gene-edited lines, describe the editor used, the endogenous sequence targeted for editing, the targeting guide RNA sequence (if applicable) and how the editor was applied.*
Authentication	*Describe any authentication procedures for each seed stock used or novel genotype generated. Describe any experiments used to assess the effect of a mutation and, where applicable, how potential secondary effects (e.g. second site T-DNA insertions, mosaicism, off-target gene editing) were examined.*